Electromagnetic turbulence in EAST plasmas with internal transport barrier

Yuehao Ma[1], Pengfei Liu[2], Jian Bao[2], Zhihong Lin[3] and Huishan Cai[1,*]

[1]CAS Key Laboratory of Frontier Physics in Controlled Nuclear Fusion, School of Nuclear Sciences and Technology, University of Science and Technology of China, Hefei 230026, China

[2]Institute of Physics, Chinese Academy of Sciences, Beijing 100190, China

[3]Department of Physics and Astronomy, University of California, Irvine, California 92697, United States of America

E-mail: hscai@mail.ustc.edu.cn

Abstract.

In this study, global nonlinear electromagnetic gyrokinetic simulations are conducted to investigate turbulence in the internal transport barrier (ITB) region of the EAST discharge with weakly reversed magnetic shear. Linear simulations reveal two dominant ion temperature gradient (ITG) modes: a higher frequency mode at the $q = 1$ surface, which dominates in the electrostatic limit, and a lower frequency mode near the $q_{\min}$ surface, which prevails under the experimental β (the ratio of plasma pressure to magnetic pressure). Therefore, electromagnetic effects play a important role in stabilizing ITG modes, and in causing the transition between the most unstable mode at different radial positions. The linear growth rate of the unstable mode in the electrostatic limit is approximately 1.25 times higher than that of the dominant mode in the electromagnetic case. However, in the electromagnetic nonlinear regime, the thermal ion heat conductivity is reduced by at least a factor of 4. This reduction primarily results from nonlinear electromagnetic effects enhancing the shearing effect of zonal flows, thereby further suppressing microturbulence. It is emphasized that the electromagnetic effect on ITG with weak magnetic shear should be included to accurately calculate the turbulent transport.

1. Introduction

Microturbulence plays a critical role in the anomalous transport of heat and particles in magnetically confined plasmas [1–3]. In general, the ion temperature gradient (ITG) turbulence primarily drives anomalous ion heat transport in the tokamak plasmas [4, 5]. The kinetic ballooning mode (KBM) [6–8], an electromagnetic instability that is destabilized at high plasma β, where β represents the ratio of plasma pressure to magnetic pressure. Suppression of these turbulence reduces core plasma transport and facilitates the formation of internal transport barrier (ITB), which are important for achieving advanced tokamak operational scenarios [9, 10].

Many factors contribute to the stabilization of turbulence in the core region of tokamak plasmas. For example, magnetic geometry effects such as reversed magnetic shear or the Shafranov shift, can modify the linear growth rates of instabilities [11–13]. Additionally, the parallel ion transit term provides further stabilization to toroidal ITG modes, particularly in core regions with small safety factor [14, 15]. Gyrokinetic simulations and experiments have demonstrated that energetic particles (EPs) generated by auxiliary heating schemes can beneficially impact ITG turbulence transport [16–19]. Many of these stabilizing factors are captured in electrostatic case; however, electromagnetic global gyrokinetic simulations are essential for accurately studying turbulent transport, as finite β can stabilize turbulence through magnetic field line bending as plasma beta increases [5, 20–24].

Recently, simulation studies of electromagnetic turbulence and experiments have been conducted in devices such as DIII-D, JET, ASDEX Upgrade, KSTAR and HL-2A [25–32]. Global gyrokinetic simulations find the electromagnetic effects greatly reduce the ITG induced thermal ion heat transport by a factor of 10 in DIII-D plasmas [25]. It has been found that energy transport driven by ITG turbulence does not decrease with increasing plasma β [33, 34]. Moreover, the electromagnetic stabilization becomes notably effective under conditions of low global magnetic shear [17, 29, 33, 35]. The formation of ITB in the EAST often benefits from configurations characterized by weakly reversed magnetic shear [36, 37], where electromagnetic effects likely play a significant role. Therefore, it is necessary to conduct gyrokinetic simulations that incorporate electromagnetic effects in the EAST ITB plasmas. In this work, we performed global simulations of electromagnetic turbulence using the first-principle gyrokinetic toroidal code (GTC) [38] based on EAST discharge [37]. Electromagnetic effects significantly suppress the higher frequency ITG mode that dominates in the electrostatic case. Hence, a lower frequency ITG near the $q_{\min}$ surface becomes dominant at the experimental β, and the ion heat conductivity is reduced by a factor of 4 relative to the electrostatic limit. The presence of EPs results in slightly reduced linear growth rates of ITG instability and induced zonal flows.

This paper is organized as follows: The physics model and simulation parameters are presented in subsections 2.1 and 2.2, respectively. Linear simulation results are discussed in subsection 2.3, while turbulence nonlinear saturation and transport are analyzed in

subsection 2.4. Finally, the summary and discussions are provided in section 3.

2. GTC simulation results of EAST ITB plasmas

2.1. Physical model in GTC

The GTC is a particle-in-cell (PIC) code developed to simulate plasma behavior and turbulence transport in fusion reactors. Over time, GTC has incorporated several key physical models, including the kinetic electron response [39], electromagnetic modeling [40], equilibrium current [41], and compressional magnetic perturbations [42]. The electromagnetic capability of GTC is implemented using a fluid-kinetic hybrid electron model [40, 43]. In this model, the electron response is separated into adiabatic and nonadiabatic components, with the adiabatic part solved by massless fluid response, and the nonadiabatic part solved using the drift-kinetic equation. The fluid-kinetic hybrid model has been successfully verified for microturbulence [41, 44], Alfvén eigenmodes [45], and current or pressure-driven MHD modes [46, 47], further establishing GTC as a powerful tool for simulating multi-scale [48] plasma physics in fusion devices.

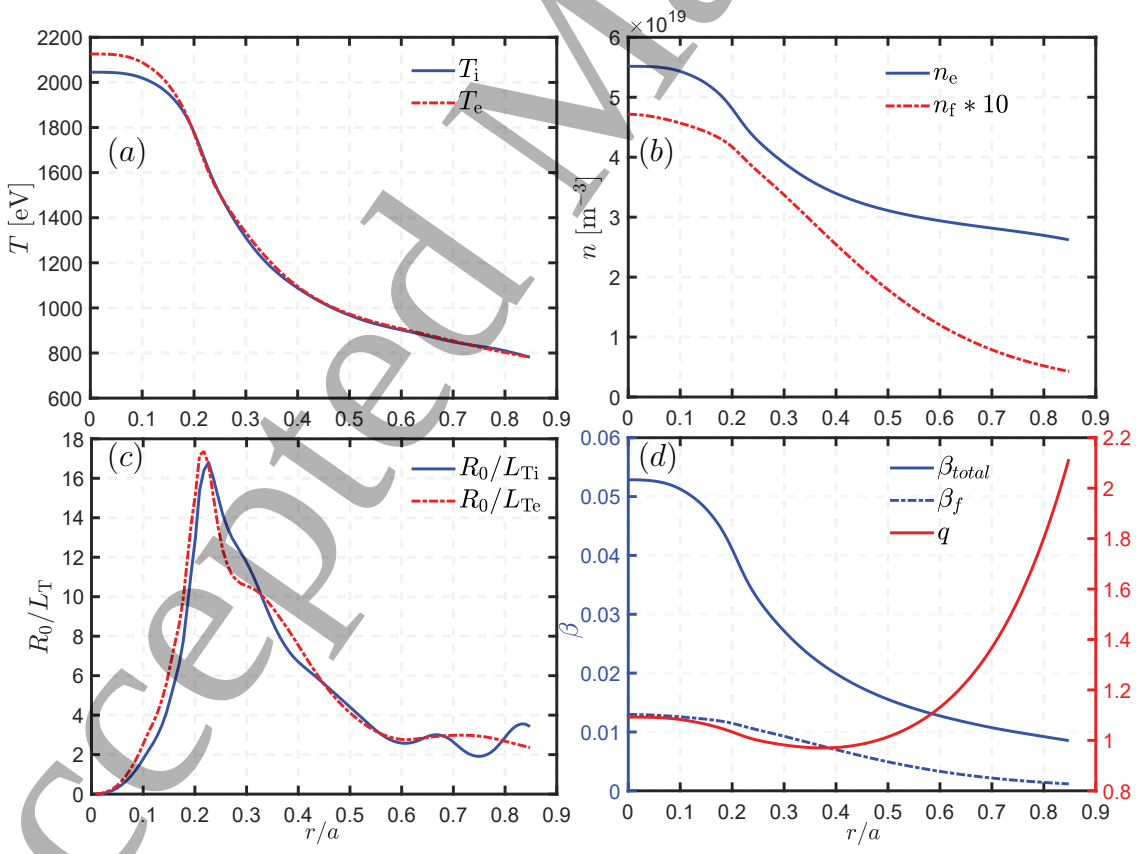

Figure 1: Plasma radial profiles in EAST discharge #93890: (a) displays temperatures T, (b) density n, (c) inverse temperature scale length R_0/L_T, and (d) the safety factor q along with the ratio of plasma pressure to magnetic pressure $\beta = 8\pi nT/B_0^2$. Subscripts i, e, and f correspond to ions, electrons, and energetic ions (fast ions), respectively.

2.2. Simulation parameters

The equilibrium of EAST tokamak discharge #93890 at 5000 ms [37], characterized by a weakly reversed magnetic shear q profile and ITBs in both ion density and temperature profiles, was previously detailed in our electrostatic turbulence study [49,50]. Building on this foundation, our current work advances into electromagnetic simulations, with figure 1 showing the plasma equilibrium. The major radius on the magnetic axis is $R_0 = 1.91$ m, and on-axis magnetic field amplitude is $B_0 = 1.49$ T. Notably, regions exhibiting ITBs are identified approximately within $r/a < 0.4$. As shown in figure 1(b), the density profile of energetic particles was computed using the NUBEAM module integrated into the ONETWO transport solver [51], with the neutral beam injection configured at an energy of approximately 50 keV. A power balance analysis has also been carried out using the ONETWO code, through which the ion thermal transport can be calculated [37]. The temperature profile of the energetic ions, equivalently calculated using a slowing-down distribution, is assumed to be radially uniform with $T_f = 15$ keV. Furthermore, this experimental scenario based on the low q_{95} operation regime exhibits a high plasma beta, as shown in figure 1(d). As beta increases, electromagnetic effects, including the finite beta effect, become more significant and cannot be neglected when analyzing plasma transport. Therefore, electromagnetic gyrokinetic simulations are essential to understand the role of these effects in determining the transport properties of the EAST ITB plasma.

2.3. Linear simulation results

In our previous electrostatic studies [49], we identified the ITG mode as the dominant instability in the ITB region, localized at the maximum ion temperature gradient and the $q = 1$ surface, with simulations incorporating both adiabatic and kinetic electron models. In this work, all electromagnetic simulations employ the kinetic electron model, incorporating the kinetic effects of the electron response. The characteristics of the ITG mode vary significantly across radial positions due to differences in equilibrium profiles and magnetic geometry. Thus, by strategically restricting the simulation domain to localized regions, we can identify both the dominant and subdominant ITG modes. Figure 2(a) displays the expermental β_i and q profiles, with β_{i0} on axis reaching approximately 2.02%. Two vertical dashed lines indicate the positions of two dominant ITG modes. One higher frequency ITG mode is located at the $q = 1$ surface with $r_1/a = 0.25$, where R_0/L_{Ti} is maximal and the experimental β_{i,r_1} is 1.1%, prevailing in the electrostatic limit [49]. However, a lower frequency ITG mode near the $q_{\min}$ surface at $r_2/a = 0.35$ is dominant at the experimental plasma beta. These modes are discussed in detail below.

The properties of instability and their dependence on β_i are investigated by changing the electron density, while the gradient of electron density is kept unchanged. This results in a vertical shift of the β_i profile. In the simulation results shown in figure 2(b), the negative mode frequency indicates that the mode propagates in the

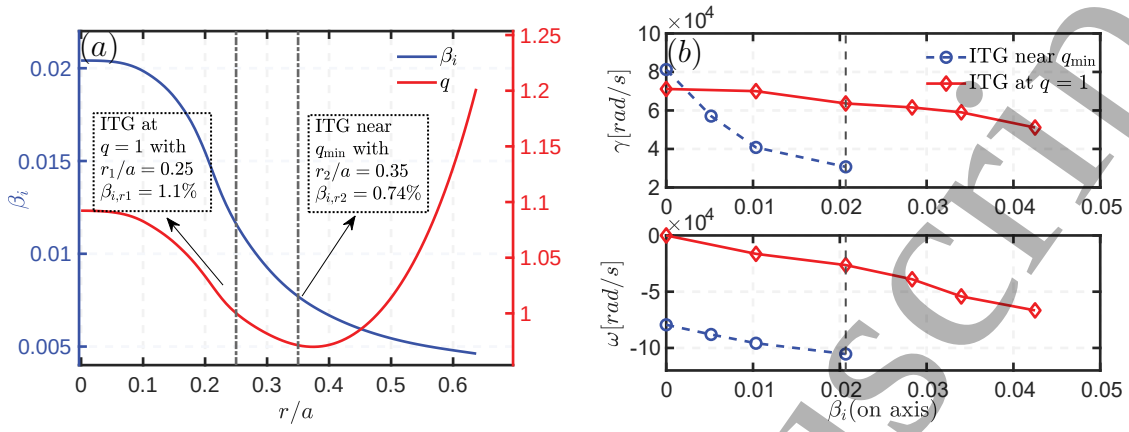

Figure 2: (a) shows the profiles of $\beta_i = 8\pi n_i T_i / B_0^2$ and q. The linear growth rate γ (top panel) and real frequency ω (bottom panel) are displayed in (b) with torodial mode number $n = 20$. The blue circular curve represents the mode at the $q = 1$ surface, while the red diamond-shaped curve corresponds to the mode located near $q_{\min}$, each as a function of β_i on axis. Different β_i values are obtained by varying the electron density ($n_e = n_i$) while keeping the density gradient unchanged. The vertical dashed lines in (b) indicate the experimental value of β_i on axis.

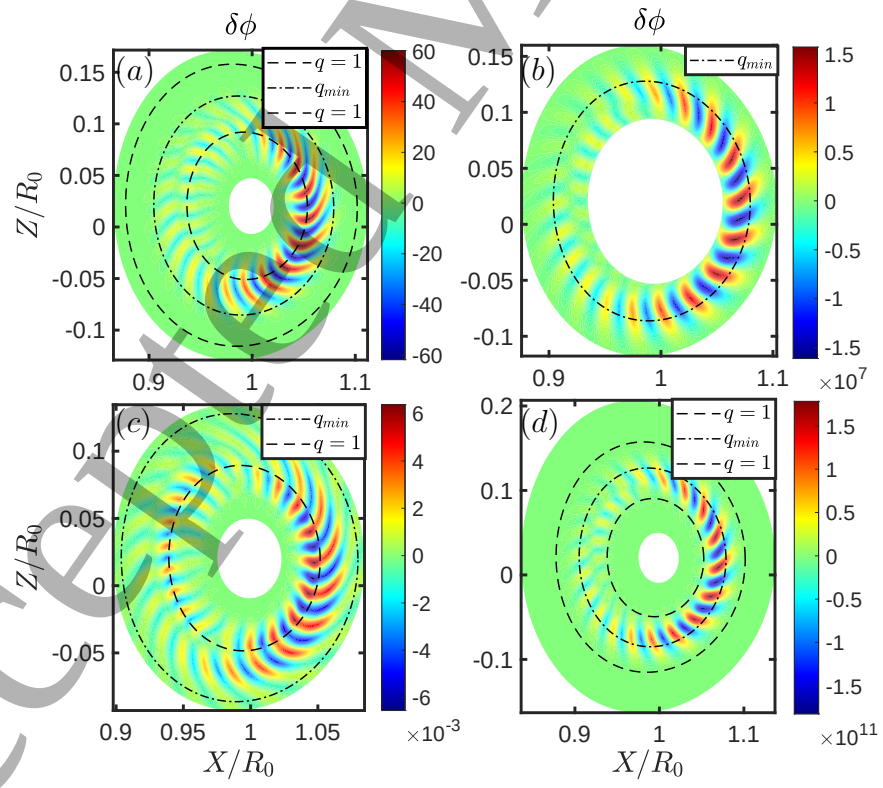

Figure 3: Mode structures of the electrostatic potential $\delta\phi$ with $n = 20$ obtained from electrostatic (top panel) and electromagnetic (bottom panel) linear simulations. Panels (a) and (c) show ITG modes at the $q = 1$ surface, while panels (b) and (d) show ITG mode near the $q_{\min}$ surface.

direction of the ion diamagnetic drift. In the electrostatic case, the ITG mode at the $q = 1$ surface is the most unstable mode in the ITB region [49], with the mode structure of $\delta\phi$ shown in figure 3(a). However, as the β_{i0} increases, the growth rate of this mode decreases significantly, with the corresponding mode structure displayed in figure 3(c). In contrast, the lower frequency ITG mode near the $q_{\min}$ surface, with the mode structure shown in figures 3(b) and (d), exhibits a smaller reduction in growth rate as β_{i0} increases. Once the β_{i0} exceeds 0.5%, this higher frequency ITG mode is no longer dominant. Thus, at the experimental plasma beta, the mode near $q_{\min}$ becomes the dominant instability in the ITB region. If only electrostatic simulations are considered, the transition between the most unstable mode at the different radial position may be missed. This phenomenon can be understood from the critical condition for electromagnetic stabilization of the ITG instability, typically characterized by $\beta_{\rm crit} \sim 1/q^2 L_{T_i}/R_0$ [5, 24]. At the $q = 1$ surface, the inverse temperature scale length R_0/L_{T_i} (shown in figure 1(c)) tends to be larger compared to its value at the $q_{\min}$ surface, resulting in a correspondingly smaller critical β. Hence, finite β effects can more effectively stabilize the ITG mode at locations with a larger temperature gradient, requiring only a lower β_i to achieve a substantial reduction in the linear growth rate. On the other hand, in the Cyclone Base Case (CBC) [52], the growth rate of ITG modes slightly decreases with increasing β_i with the normal magnetic shear q profile [23]. However, the finite β effects significantly influence the ITG instability in the weakly reversed magnetic shear configuration of the EAST ITB plasma.

Next, we focus primarily on the ITG mode located near the $q_{\min}$ surface. The ITG mode with toroidal mode number $n = 25$ at this location is unstable at low β_i, with a small real frequency, as shown in figure 4(a). The vertical dashed lines in figure 4(a) indicate the experimental vaule of β_{i,r_2} at the mode location. However, when β_{i,r_2} exceeds approximately 3%, the KBM instability becomes unstable and its real frequency is significantly greater than that of the ITG mode. It is similar to the electromagnetic ITG and KBM instabilities observed in the CBC [23] and DIII-D tokamak pedestal studies [44]. Figures 5(a) and (c) illustrate that both ITG and KBM display ballooning structures in the electrostatic potential $\delta\phi$. The ITG perturbation exhibits a more pronounced ballooning angle, indicating a significant deviation from the out-midplane. In contrast, the KBM eigenmode structure is closer to the ideal ballooning mode. Figure 5(b) illustrates the ITG polarization, where the parallel electrostatic field $E_\parallel^{\rm ES} = -\mathbf{b}_0 \cdot \nabla\delta\phi$ is almost identical to the net parallel electric field $E_\parallel^{\rm Net} = -\mathbf{b}_0 \cdot \nabla\delta\phi - (1/c)\partial_t \delta A_\parallel$ indicating the quasi-electrostatic properties of the ITG mode. In contrast, as shown in figure 5(d) for the KBM, the amplitude of $E_\parallel^{\rm Net}$ is significantly smaller than that of $E_\parallel^{\rm ES}$ for all poloidal harmonics which leads to the predominantly Alfvénic polarization [53]. Finally, figure 4(b) presents the dispersion relation, showing the dependence of the linear growth rate and real frequency on the poloidal wavenumber (or equivalently, toroidal mode number n). The most unstable toroidal mode $n = 25$ corresponds to a poloidal wavenumber $k_\theta \approx 1.9\,{\rm cm}^{-1}$, close to values measured by poloidal correlation reflectometry (PCR) [54].

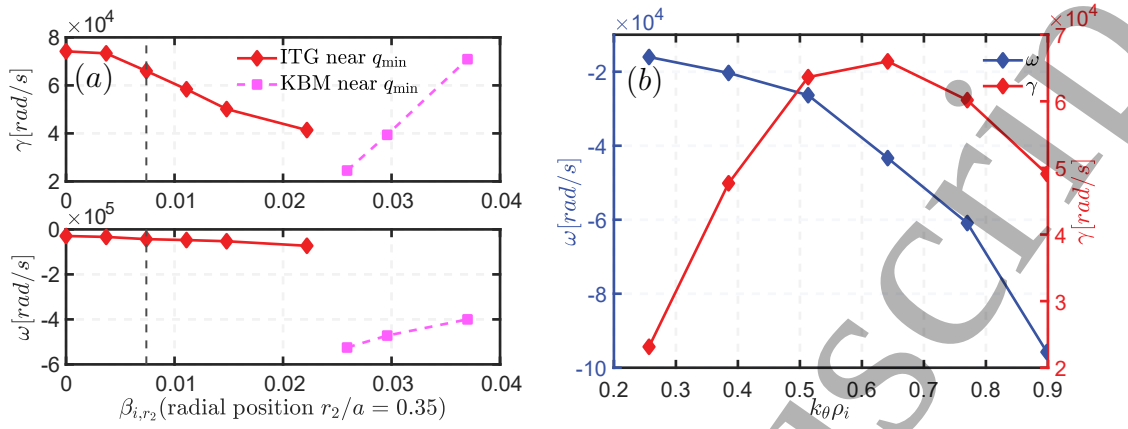

Figure 4: (a) The linear growth rate γ (top panel) and real frequency ω (bottom panel) are shown for the mode located near $q_{\min}$ with $n = 25$, as a function of β_{i,r_2} which is evaluated at mode location. (b) Dependence of the ITG mode near the $q_{\min}$ surface growth rate and real frequency on the poloidal wavelength $k_\theta \rho_i$ (corresponding to toroidal mode numbers $n = 10, 15, \ldots, 35$).

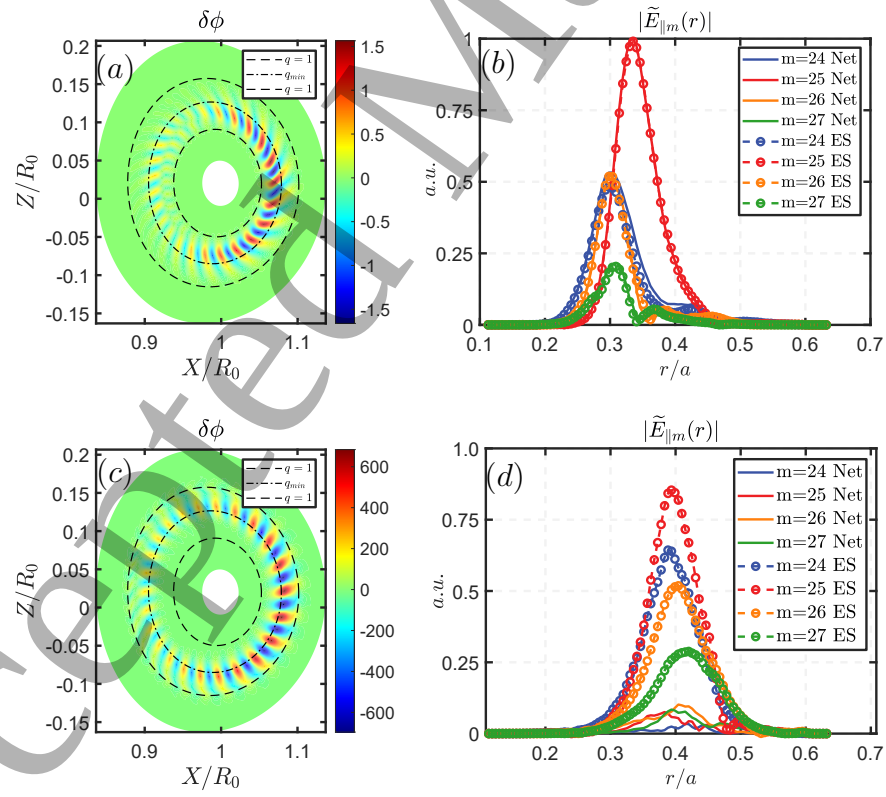

Figure 5: Mode structures of the $n = 25$ ITG mode (top panel) at $\beta_i = 1.11\%$ and the KBM mode (bottom panel) at $\beta_i = 3.7\%$: (a) and (c) show the poloidal contour plots of the $\delta\phi$, while (b) and (d) display the poloidal harmonics radial profiles of the parallel electric field $E_\parallel$. In (b) and (d), the solid lines with circles represent $E_\parallel^{\rm ES} = -\mathbf{b}_0 \cdot \nabla \delta\phi$, and the solid lines correspond to $E_\parallel^{\rm Net} = -\mathbf{b}_0 \cdot \nabla \delta\phi - (1/c)\partial_t \delta A_\parallel$.

2.4. Nonlinear simulation results

In this subsection, global electromagnetic multi-n nonlinear simulations are conducted to investigate the saturation and transport mechanisms of the ITG mode in the ITB region. All nonlinear electromagnetic simulations are performed at the experimental value of β_i. The kinetic electron model is employed to consider the kinetic effects of electrons. The simulations include toroidal modes $n = 10, 11, 12, \ldots, 39$. Figures 6(a) and (b) illustrate the time evolution of the electrostatic potential $\delta\phi$ and parallel vector potential $\delta A_\parallel$ from the electromagnetic ITG simulation. Linearly most unstable ITG modes (e.g., $n = 25$) are firstly driven and dominate the early stage. The $\delta\phi_{n=25}$ and $\delta A_{\parallel n=25}$ exhibit exponential growth at the linear growth rate $\gamma_{n=25}$. In both the linear and intermediate regimes, $\delta\phi_{00}$ and $\delta A_{\parallel 00}$ grow exponentially at a growth rate $\gamma_{n,m=0} \approx 2\,\gamma_{n=25}$. This

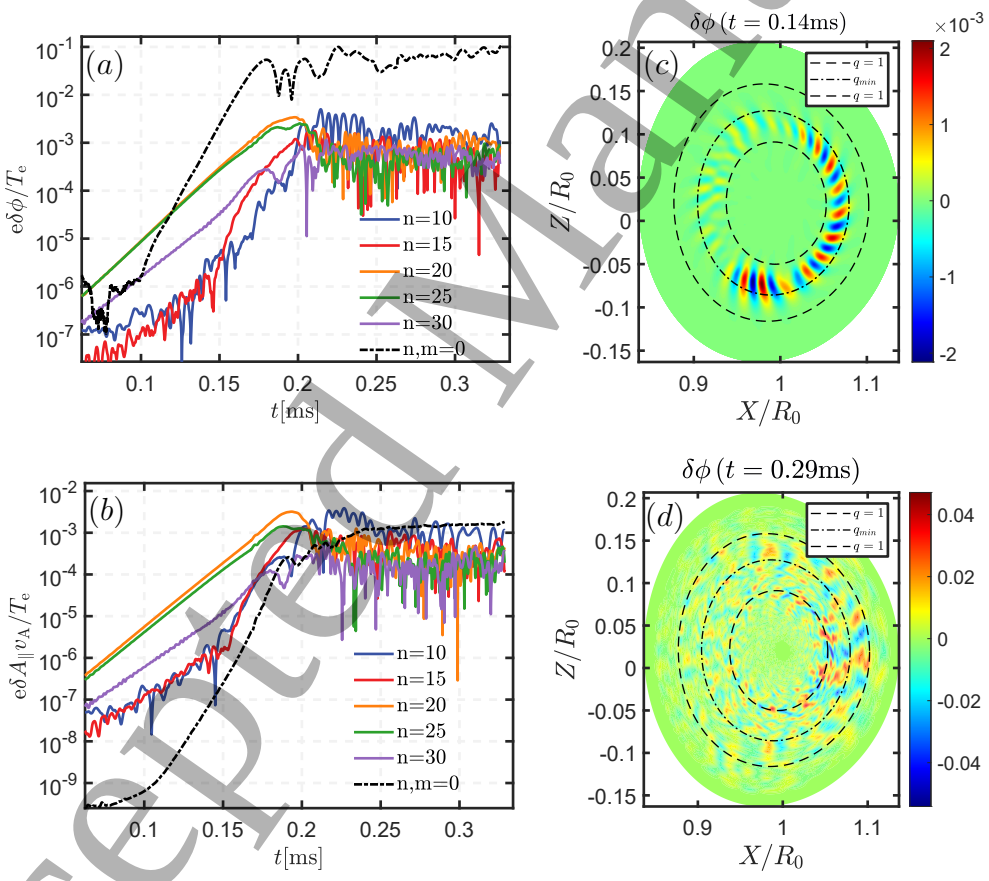

Figure 6: Time evolution of the perturbed electrostatic potential $\delta\phi$ and parallel vector potential $\delta A_\parallel$ for selected toroidal n modes near the $q_{\min}$ flux surface from electromagnetic ITG simulations. The perturbed electrostatic potential and parallel vector potential are normalized as $e\delta\phi/T_e$ and $e\delta A_\parallel v_A/T_e$, respectively, where the Alfvén velocity is $v_A = B_0/\sqrt{4\pi n_{i0} m_i}$. The black dashed lines represent the zonal flow $\delta\phi_{00}$ and the zonal current $\delta A_{\parallel 00}$, both shown as root-mean-square (rms) values averaged across the simulation domain. (c) and (d): Poloidal contour plots of the electrostatic potential $\delta\phi$ during the linear and nonlinear phases, respectively.

observation suggests that the zonal fields in ITG turbulence are passively generated via the so-called beat-driven process [55]. Near 0.25 ms, the ITG turbulence saturates and settles into a steady state nonlinear regime. At this stage, the amplitude of $\delta\phi_{n=25}$ is on the order of 10^{-3}, while $\delta A_{\parallel}$ is on the order of 10^{-4}. Figure 6(c) and (d) depict the mode structure of the perturbed electrostatic potential during the linear regime and the nonlinear saturation regime, respectively. From the contour plots, it is apparent that high n modes (e.g., $n = 20$ and $n = 25$) dominate the electromagnetic ITG instability and are located between $q_{\min}$ and $q = 1$ in the linear phase. In contrast, low n modes dominate the nonlinear phase and the turbulence spreads across the entire radial domain. The time history of the $\delta\phi$ and $\delta A_{\parallel}$ also show that once nonlinear saturation is reached, the amplitude of the low n modes becomes larger than that of the high n modes.

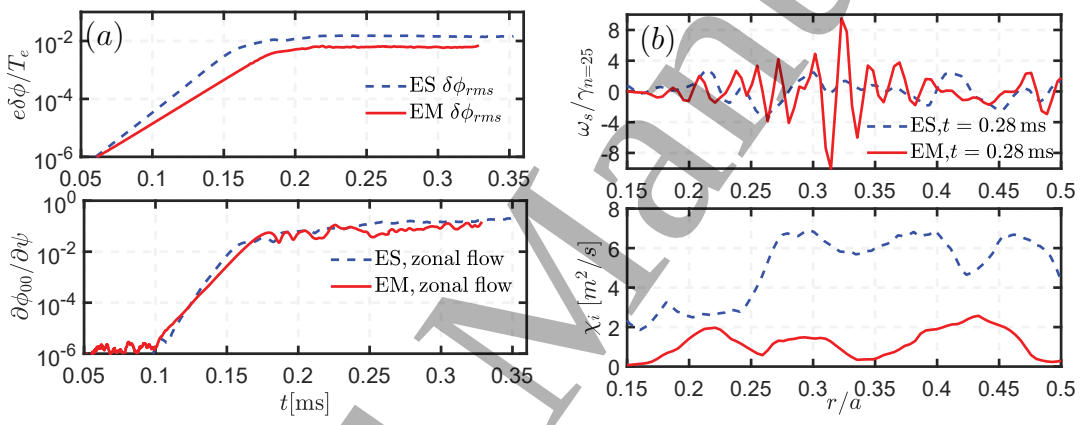

Figure 7: (a) Time evolution of the volume-averaged turbulence intensity $\delta\phi$ (top panel) and zonal flow (bottom panel) from electrostatic (dashed lines) and electromagnetic (solid lines) simulations. (b) The radial structures of the zonal flow shearing rate ω_s (top panel) and thermal ion heat conductivity (bottom panel) in the nonlinear phase for both electrostatic and electromagnetic cases, and the shearing rate normalized by the growth rate of the ITG mode with $n = 25$ near $q_{\min}$.

Figure 7(a) shows the time evolution of the volume-averaged perturbed electrostatic potential as well as the zonal flows for both electrostatic and electromagnetic ITG simulations. The turbulence intensity in the electromagnetic case is roughly three times smaller than that in the electrostatic case. The zonal flows amplitude is slightly smaller in the electromagnetic case. However, as shown in figure 7(b), the zonal flows shearing rate $\omega_s = -(RB_\theta)^2/B_0\,\partial^2\phi_{00}/\partial\psi^2$ [56, 57] is significantly larger in the electromagnetic case. Figure 7(b) also show the radial profile of thermal ion heat conductivity from both electrostatic and electromagnetic ITG simulations. The radial profiles of the thermal ion heat conductivity at the nonlinear saturation stage reveal that $\chi_i \gtrsim 1.5\,\mathrm{m}^2/\mathrm{s}$ in the electromagnetic case, which is significantly smaller than $\chi_i \sim 6\,\mathrm{m}^2/\mathrm{s}$ observed in the electrostatic case. It is observed that the ion heat conductivity is smaller in regions with higher shearing rate, indicating that the zonal flow shearing rate plays an important role

in suppressing microturbulence. Notably, the radial region of reduced ion heat diffusivity χ_i and elevated normalized zonal flows shearing rate in figure 7(b) broadly coincides with the region of large R_0/L_{Ti} shown in figure 1(c). This spatial correlation suggests that enhanced zonal flows shear can regulate turbulence even where the linear drive is strong. The thermal ion heat conductivity obtained from GTC agrees in magnitude with the results from the power balance analysis performed using the ONETWO code [37]. In summary, linear results indicate that the growth rate of the unstable mode in the electrostatic limit is approximately 1.25 times higher than that in the electromagnetic case. However, in the nonlinear phase of electromagnetic ITG, the transport coefficient is reduced by at least a factor of 4. The reduction is driven mainly by enhanced zonal flows shear that suppresses microturbulence during the nonlinear phase, with electromagnetic effects further reducing the linear growth rate.

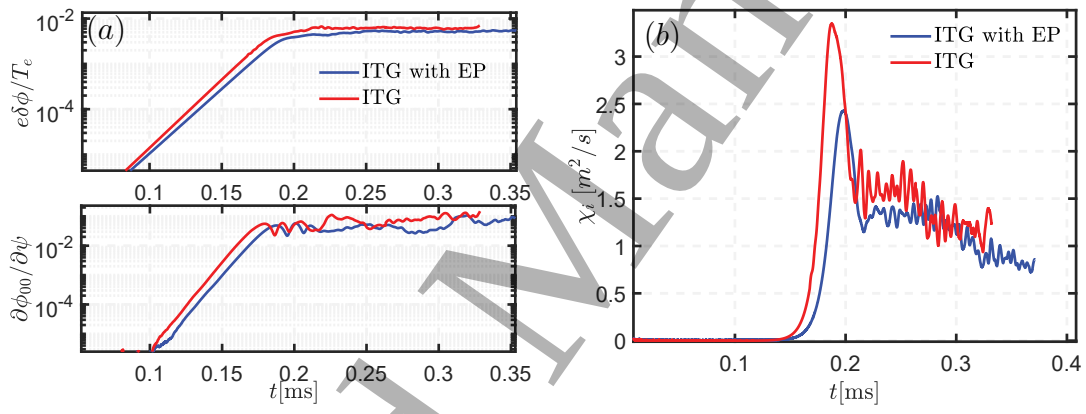

Figure 8: (a) Time evolution of the volume-averaged turbulence intensity $\delta\phi$ (top panel) and the zonal flow (bottom panel), and (b) the thermal ion heat conductivity, all obtained from electromagnetic ITG simulations with EPs (the blue line) and without EPs (the red line).

Finally, the impact of energetic particles on electromagnetic ITG turbulence is investigated. As shown in figure 8, the presence of EPs leads to a slight reduction in both the ITG linear growth rate and the induced zonal flow. Moreover, at the nonlinear stage, the turbulence saturation level remains nearly unchanged, leading to only minor modifications in the ion heat conductivity. Overall, these findings indicate that EPs exert a stabilizing influence on ITG turbulence. This slight stabilization is likely attributed to the dilution effect of EPs ($n_f/n_e \lesssim 0.1$) and their finite β effect [16, 58]. Evidently, the direct impact of EPs on ITG turbulence is minimal in our case. In the next step, we will explore the excitation of fishbone modes by EPs and their interaction with ITG turbulence through global nonlinear gyrokinetic cross-scale coupling simulations, aiming to further uncover the mechanisms underlying ITB formation.

3. Conclusions and discussions

In this paper, global gyrokinetic simulations are performed to investigate electromagnetic turbulence in the ITB region of an EAST tokamak discharge (#93890). GTC linear simulation results reveal the transition of the most unstable ITG mode at different radial positions due to the finite β effects. Specifically, two dominant ITG modes at different radial positions: a higher frequency mode located at the $q = 1$ surface, which dominates in the electrostatic limit, and a lower frequency mode found near the $q_{\min}$ surface, which prevails in the electromagnetic regime. When electromagnetic effects are included, the ITG instability at the $q = 1$ surface is effectively suppressed, while the ITG mode near the $q_{\min}$ surface exhibits a smaller reduction in growth rate. Finite β effects can more effectively stabilize the ITG mode at locations with a larger temperature gradient. It is therefore expected that electromagnetic stabilization effects may provide a negative feedback mechanism that regulates the turbulence driven by increasing temperature gradient during ITB formation.

Electromagnetic multi-n nonlinear simulations primarily focus on the transport levels of turbulence. A comparison between electrostatic and electromagnetic turbulence demonstrates that including electromagnetic effects reduces the ion heat conductivity by at least a factor of 4. On one hand, electromagnetic effects play a important role in reducing the linear growth rate. On the other hand, although the zonal flows amplitude is smaller in the electromagnetic case compared to the electrostatic limit, the shearing effect of the zonal flows is significantly larger, resulting in a stronger suppression of microturbulence during the nonlinear phase. In this case, EPs exert a slight stabilizing influence on ITG turbulence, likely due to the dilution effect and finite β contribution of EPs. In future work, we will study electromagnetic turbulent transport using gyrokinetic simulations under self-consistent magnetohydrodynamic equilibrium for each β.

Acknowledgments

The authors acknowledge B. Zhang and T. Zhang for providing experimental data. This work was supported by the National MCF Energy R&D Program of China (Grant Nos. 2024YFE03050002), the Strategic Priority Research Program of Chinese Academy of Sciences (Grant Nos. XDB0790202 and XDB0500302), and National Natural Science Foundation of China (Grant Nos. 12025508 and 12275351). The numerical calculations in this paper were performed on the Hefei Advanced Computing Center, National Tianjin Supercomputing Center, and the Supercomputing Center of the University of Science and Technology of China.

References

[1] W Horton. Drift waves and transport. *Reviews of Modern Physics*, 71(3):735, 1999.
[2] Wendell Horton. *Turbulent transport in magnetized plasmas*. World Scientific, 2012.

[3] Jan Weiland and Anatoly Zagorodny. Drift wave theory for transport in tokamaks. *Reviews of Modern Plasma Physics*, 3(1):8, 2019.

[4] Ft Romanelli. Ion temperature-gradient-driven modes and anomalous ion transport in tokamaks. *Physics of Fluids B: Plasma Physics*, 1(5):1018–1025, 1989.

[5] JY Kim, W Horton, and JQ Dong. Electromagnetic effect on the toroidal ion temperature gradient mode. *Physics of Fluids B: Plasma Physics*, 5(11):4030–4039, 1993.

[6] WM Tang, JW Connor, and RJ Hastie. Kinetic-ballooning-mode theory in general geometry. *Nuclear Fusion*, 20(11):1439, 1980.

[7] Akira Hirose, L Zhang, and M Elia. Higher order collisionless ballooning mode in tokamaks. *Physical review letters*, 72(25):3993, 1994.

[8] Ge Dong, Jian Bao, Amitava Bhattacharjee, and Zhihong Lin. Nonlinear saturation of kinetic ballooning modes by zonal fields in toroidal plasmas. *Physics of Plasmas*, 26(1), 2019.

[9] JW Connor, T Fukuda, X Garbet, C Gormezano, V Mukhovatov, M Wakatani, et al. A review of internal transport barrier physics for steady-state operation of tokamaks. *Nuclear Fusion*, 44(4):R1, 2004.

[10] Katsumi Ida and Takaaki Fujita. Internal transport barrier in tokamak and helical plasmas. *Plasma Physics and Controlled Fusion*, 60(3):033001, 2018.

[11] C Kessel, Jf Manickam, G Rewoldt, and WM Tang. Improved plasma performance in tokamaks with negative magnetic shear. *Physical Review Letters*, 72(8):1212, 1994.

[12] TM Antonsen Jr, JF Drake, PN Guzdar, AB Hassam, YT Lau, CS Liu, and SV Novakovskii. Physical mechanism of enhanced stability from negative shear in tokamaks: Implications for edge transport and the l-h transition. *Physics of Plasmas*, 3(6):2221–2223, 1996.

[13] C Bourdelle, GT Hoang, X Litaudon, CM Roach, and Tuomas Tala. Impact of the α parameter on the microstability of internal transport barriers. *Nuclear fusion*, 45(2):110, 2005.

[14] RR Dominguez and MN Rosenbluth. Local kinetic stability analysis of the ion temperature gradient mode. *Nuclear fusion*, 29(5):844, 1989.

[15] JQ Dong, W Horton, and JY Kim. Toroidal kinetic η i-mode study in high-temperature plasmas. *Physics of Fluids B: Plasma Physics*, 4(7):1867–1876, 1992.

[16] G Tardini, J Hobirk, VG Igochine, CF Maggi, P Martin, D McCune, AG Peeters, ACC Sips, A Stäbler, J Stober, et al. Thermal ions dilution and itg suppression in asdex upgrade ion itbs. *Nuclear fusion*, 47(4):280, 2007.

[17] Jonathan Citrin, F Jenko, P Mantica, D Told, C Bourdelle, J Garcia, JW Haverkort, GMD Hogeweij, Thomas Johnson, and MJ Pueschel. Nonlinear stabilization of tokamak microturbulence by fast ions. *Physical review letters*, 111(15):155001, 2013.

[18] A Di Siena, R Bilato, T Görler, A Banón Navarro, E Poli, V Bobkov, D Jarema, E Fable, C Angioni, Ye O Kazakov, et al. New high-confinement regime with fast ions in the core of fusion plasmas. *Physical Review Letters*, 127(2):025002, 2021.

[19] Yong-Su Na, TS Hahm, PH Diamond, A Di Siena, J Garcia, and Z Lin. How fast ions mitigate turbulence and enhance confinement in tokamak fusion plasmas. *Nature Reviews Physics*, pages 1–13, 2025.

[20] J Candy. Beta scaling of transport in microturbulence simulations. *Physics of Plasmas*, 12(7), 2005.

[21] Moritz J Pueschel, M Kammerer, and F Jenko. Gyrokinetic turbulence simulations at high plasma beta. *Physics of Plasmas*, 15(10), 2008.

[22] MJ Pueschel and F Jenko. Transport properties of finite-β microturbulence. *Physics of Plasmas*, 17(6), 2010.

[23] I Holod and Z Lin. Verification of electromagnetic fluid-kinetic hybrid electron model in global gyrokinetic particle simulation. *Physics of Plasmas*, 20(3), 2013.

[24] A Zocco, P Helander, and JW Connor. Magnetic compressibility and ion-temperature-gradient-driven microinstabilities in magnetically confined plasmas. *Plasma Physics and Controlled Fusion*, 57(8):085003, 2015.

[25] P Liu, X Wei, Z Lin, WW Heidbrink, G Brochard, GJ Choi, JH Nicolau, and W Zhang. Cross-scale interaction between microturbulence and meso-scale reversed shear alfvén eigenmodes in diii-d plasmas. *Nuclear Fusion*, 64(7):076007, 2024.

[26] P Mantica, C Angioni, C Challis, G Colyer, Lorenzo Frassinetti, N Hawkes, Thomas Johnson, M Tsalas, PC Devries, Jan Weiland, et al. A key to improved ion core confinement in the jet tokamak:<? format?> ion stiffness mitigation due to combined plasma rotation and low magnetic shear. *Physical review letters*, 107(13):135004, 2011.

[27] L Vermare, F Ryter, C Angioni, AG Peeters, J Stober, R Bilato, LD Horton, B Kurzan, CF Maggi, H Meister, et al. Study of the β dependence of confinement and heat transport in asdex upgrade. *Nuclear fusion*, 47:490–497, 2007.

[28] H Doerk, A Bock, A Di Siena, E Fable, T Görler, F Jenko, J Stober, ASDEX Upgrade Team, et al. Turbulence in high-beta asdex upgrade advanced scenarios. *Nuclear Fusion*, 58(1):016044, 2017.

[29] J Citrin, J Garcia, T Görler, F Jenko, P Mantica, D Told, C Bourdelle, DR Hatch, GMD Hogeweij, Thomas Johnson, et al. Electromagnetic stabilization of tokamak microturbulence in a high-β regime. *Plasma Physics and Controlled Fusion*, 57(1):014032, 2014.

[30] J Garcia, C Challis, J Citrin, H Doerk, G Giruzzi, T Görler, F Jenko, P Maget, and JET Contributors. Key impact of finite-beta and fast ions in core and edge tokamak regions for the transition to advanced scenarios. *Nuclear Fusion*, 55(5):053007, 2015.

[31] H Han, SJ Park, Choongki Sung, J Kang, YH Lee, J Chung, Taik Soo Hahm, B Kim, J-K Park, JG Bak, et al. A sustained high-temperature fusion plasma regime facilitated by fast ions. *Nature*, 609(7926):269–275, 2022.

[32] JQ Xu, XD Peng, W Chen, GZ Hao, JQ Li, HP Qu, ZJ Li, XX He, YG Li, M Jiang, et al. Impact of fast ions on microturbulence and zonal flow dynamics in hl-2a internal transport barriers. *Nuclear Fusion*, 63(12):126026, 2023.

[33] A Ishizawa, D Urano, Y Nakamura, S Maeyama, and T-H Watanabe. Persistence of ion temperature gradient turbulent transport at finite normalized pressure. *Physical Review Letters*, 123(2):025003, 2019.

[34] M Niiro, A Ishizawa, Y Nakamura, S Maeyama, and TH Watanabe. Plasma beta dependence of ion temperature gradient driven turbulence influenced by shafranov shift. *Plasma Physics and Controlled Fusion*, 65(6):065004, 2023.

[35] Jonathan Citrin and Paola Mantica. Overview of tokamak turbulence stabilization by fast ions. *Plasma Physics and Controlled Fusion*, 65(3):033001, 2023.

[36] X Gao, L Zeng, MQ Wu, T Zhang, Y Yang, TF Ming, X Zhu, YM Wang, HQ Liu, Q Zang, et al. Experimental progress of hybrid operational scenario on east tokamak. *Nuclear Fusion*, 60(10):102001, 2020.

[37] B Zhang, X Gong, J Qian, L Zeng, LQ Xu, YM Duan, JY Zhang, YC Hu, TQ Jia, P Li, et al. Progress on physics understanding of improved confinement with fishbone instability at low q 95< 3.5 operation regime in east. *Nuclear Fusion*, 62(12):126064, 2022.

[38] Zhihong Lin, Taik Soo Hahm, WW Lee, William M Tang, and Roscoe B White. Turbulent transport reduction by zonal flows: Massively parallel simulations. *Science*, 281(5384):1835–1837, 1998.

[39] Z Lin, Y Nishimura, Y Xiao, I Holod, WL Zhang, and L Chen. Global gyrokinetic particle simulations with kinetic electrons. *Plasma Physics and Controlled Fusion*, 49(12B):B163, 2007.

[40] I Holod, WL Zhang, Y Xiao, and Z Lin. Electromagnetic formulation of global gyrokinetic particle simulation in toroidal geometry. *Physics of Plasmas*, 16(12):122307, 2009.

[41] W Deng, Z Lin, and I Holod. Gyrokinetic simulation model for kinetic magnetohydrodynamic processes in magnetized plasmas. *Nuclear Fusion*, 52(2):023005, 2012.

[42] Ge Dong, Jian Bao, Amitava Bhattacharjee, Alain Brizard, Zhihong Lin, and Peter Porazik. Gyrokinetic particle simulations of the effects of compressional magnetic perturbations on drift-alfvenic instabilities in tokamaks. *Physics of Plasmas*, 24(8), 2017.

[43] Xishuo Wei, Gyungjin Choi, Guillaume Brochard, Pengfei Liu, Zhihong Lin, and Jian Bao.

Electromagnetic formulations for gtc simulation, 2021.

[44] I Holod, D Fulton, and Zhihong Lin. Microturbulence in diii-d tokamak pedestal. ii. electromagnetic instabilities. *Nuclear Fusion*, 55(9):093020, 2015.

[45] HS Zhang, Z Lin, and I Holod. Nonlinear frequency oscillation of alfvén eigenmodes in fusion plasmas. *Physical review letters*, 109(2):025001, 2012.

[46] J McClenaghan, Z Lin, I Holod, W Deng, and Z Wang. Verification of gyrokinetic particle simulation of current-driven instability in fusion plasmas. i. internal kink mode. *Physics of Plasmas*, 21(12), 2014.

[47] Guillaume Brochard, Jian Bao, Chang Liu, Nikolai Gorelenkov, G Choi, G Dong, P Liu, J Mc Clenaghan, JH Nicolau, F Wang, et al. Verification and validation of linear gyrokinetic and kinetic-mhd simulations for internal kink instability in diii-d tokamak. *Nuclear Fusion*, 62(3):036021, 2022.

[48] Pengfei Liu, Xishuo Wei, Zhihong Lin, Guillaume Brochard, GJ Choi, WW Heidbrink, JH Nicolau, and GR McKee. Regulation of alfvén eigenmodes by microturbulence in fusion plasmas. *Physical Review Letters*, 128(18):185001, 2022.

[49] Yuehao Ma, Bin Zhang, Jian Bao, Z Lin, Wenlu Zhang, Huishan Cai, and Ding Li. Electrostatic turbulence in east plasmas with internal transport barrier. *Nuclear Fusion*, 63(5):056014, 2023.

[50] Qien Jing, Yuehao Ma, Huishan Cai, and Zhihong Lin. Synergistic effect between radial electric field and magnetic shear on ion temperature gradient mode. *Nuclear Fusion*, 65(10):106037, 2025.

[51] WW Pfeiffer, RH Davidson, RL Miller, and RE Waltz. Onetwo: a computer code for modeling plasa transport in tokamaks. Technical report, General Atomics, San Diego, CA (United States), 1980.

[52] A. M. Dimits, G. Bateman, M. A. Beer, B. I. Cohen, W. Dorland, G. W. Hammett, C. Kim, J. E. Kinsey, M. Kotschenreuther, A. H. Kritz, L. L. Lao, J. Mandrekas, W. M. Nevins, S. E. Parker, A. J. Redd, D. E. Shumaker, R. Sydora, and J. Weiland. Comparisons and physics basis of tokamak transport models and turbulence simulations. *Phys. Plasmas*, 7(3):969–983, 2000.

[53] Jian Bao, WL Zhang, Ding Li, Zhihong Lin, Ge Dong, Chang Liu, HS Xie, Guo Meng, JY Cheng, Chao Dong, et al. Mas: A versatile landau-fluid eigenvalue code for plasma stability analysis in general geometry. *Nuclear Fusion*, 63(7):076021, 2023.

[54] LI Gongshun, Tao ZHANG, GENG Kangning, WEN Fei, YE Kaixuan, XU Liqing, ZHU Xiang, Xuexi ZHANG, Fubin ZHONG, ZHOU Zhen, et al. Observation of doppler shift modulated by the internal kink mode using conventional reflectometry in the east tokamak. *Plasma Science and Technology*, 26(3):034001, 2024.

[55] Liu Chen, Zhiyong Qiu, and Fulvio Zonca. On beat-driven and spontaneous excitations of zonal flows by drift waves. *Physics of Plasmas*, 31(4), 2024.

[56] KH Burrell. Effects of e× b velocity shear and magnetic shear on turbulence and transport in magnetic confinement devices. *Physics of Plasmas*, 4(5):1499–1518, 1997.

[57] TS Hahm, MA Beer, Z Lin, GW Hammett, WW Lee, and WM Tang. Shearing rate of time-dependent e × b flow. *Physics of Plasmas*, 6(3):922–926, 1999.

[58] M. Liljeström. Low frequency electrostatic instabilities in a toroidal plasma with a hot ion beam. *Nuclear Fusion*, 30(12):2611, dec 1990.